Materials Today Energy 16 (2020) 100421

Contents lists available at ScienceDirect

Materials Today Energy

journal homepage: www.journals.elsevier.com/materials-today-energy/

Influence of Kubas-type interaction of B—Ni codoped graphdiyne with hydrogen molecules on desorption temperature and storage efficiency

E.V. Anikina [a, b], A. Banerjee [c, *], V.P. Beskachko [b], R. Ahuja [a, c]

[a] Materials Theory Division, Department of Physics and Astronomy, Uppsala University, Box 516, 75120 Uppsala, Sweden
[b] Institute of Natural Sciences and Mathematics, South Ural State University, 76, Lenin Prospekt, Chelyabinsk 454014, Russia
[c] Applied Materials Physics, Department of Materials and Engineering, KTH Royal Institute of Technology, S-100 44, Stockholm, Sweden

ARTICLE INFO

Article history:
Received 17 March 2020
Received in revised form
12 April 2020
Accepted 15 April 2020
Available online 6 May 2020

Keywords:
Monolayer
2D carbon allotrope
ab initio molecular dynamics (AIMD)
Hybrid functional
vdW corrections

ABSTRACT

We have investigated functionalized 2D carbon allotrope, graphdiyne (GDY), as a promising hydrogen storage media. Density functional theory with a range of vdW corrections was employed to study Ni decoration of pristine and boron-doped GDY and the interaction of resulting structures with molecular hydrogen. We showed that boron-doped GDY is thermally stable at 300 K, though, its synthesis requires an endothermic reaction. Also, boron doping enhances Ni binding with the graphdiyne by increasing the charge transfer from Ni to GDY. Ni doping drastically influenced hydrogen adsorption energies: they rise from ~70 meV per H_2 molecule on pristine GDY to a maximum of 1.29 eV per H_2 becoming too high in value for room temperature reversible applications. Boron doping improves the situations: in this case, after Ni decoration desorption temperature estimation is ~300—500 K. Overall, each Ni adatom on B-doped GDY can bind only one H_2 molecule within the needed energy range, which gives low hydrogen uptake (~1.2 wt%). However, doping with boron led to the decrease in the value of hydrogen adsorption energy and good desorption temperature estimations, therefore, codoping of metal atoms and boron could be an effective strategy for other transition metals.

1. Introduction

With the rising rates of energy consumption, the investigations of ecologically-friendly sources of energy and ways of its redistribution are of high importance nowadays. Hydrogen is a promising energy carrier if produced from renewable sources [1,2]. However, compact, safe, and effective hydrogen storage systems, which satisfy the U.S. Department of Energy targets for on-board applications [3], are still needed. Carbon-based nanomaterials attract the attention of researchers in the field for a long time because of their porosity, low density, and low production cost [4]. Moreover, these materials exhibit good hydrogen storage capacities [5,6], though, only at cryogenic temperatures.

Novel two-dimensional (2D) carbon nanomaterials have been actively investigated since they have a potential for a high hydrogen uptake due to the high surface area. Graphdiyne (GDY), 2D carbon allotrope [7], has been predicted as the most stable diacetylenic carbon allotrope [8] and recently successfully synthesized [9]. However, molecular hydrogen interacts with the pure GDY via week van der Waals forces, and theoretical predictions showed that pure graphdiyne binds hydrogen with energy ~60—70 meV/molecule, which is too low for room-temperature reversible sorption/desorption cycles [10]. This problem could be solved by adding more active adsorption sites on the GDY surface (e.g., metal atoms).

There are two possible approaches: to add light metals to the carbon-based structure or to use heavier transition metals (TM). The former way allows us to minimize the final weight of a base structure; therefore, the resulting hydrogen uptake will be less negatively affected. And, indeed, doping with light alkali and alkali-earth elements increases hydrogen binding energy significantly due to the charge-induced polarization of hydrogen molecules (up to ~0.3 eV/molecule) [11,12]. However, even with these enhanced binding energies, desorption temperature stays considerably lower than the desired room temperature. Moreover, light metals significantly improve binding energy of not a big number of hydrogen molecules (for example, Li adsorbed on carbon nanotubes [13] or carbyne [14] influences only up to 3—4 hydrogen molecules per metal adatom). The latter approach, on the other hand, allows getting biding energies, which are closer to the chemisorption due

* Corresponding author.
E-mail address: amitava245@gmail.com (A. Banerjee).

https://doi.org/10.1016/j.mtener.2020.100421

to the Kubas-type interactions between hydrogen molecules and TM adatoms [15]. Such interactions involve the stabilization of H_2 complexes by σ-donation from the filled H—H bonding orbital into the empty *d*-orbital of a metal atom and simultaneous back-donation of electrons from the filled metal *d*-orbital into the vacant anti-bonding orbital of the H_2 molecule [16]. Such back-donation is crucial not only in stabilizing the bonding but also in a lengthening of the H—H bond (and even splitting if it is too strong) [17]. Besides, usually, transition metals can strongly bind more hydrogen molecules than light alkali metals [11,16,18].

Previously, He et al. [19] investigated GDY decoration with light transition metals (though, they did not consider hydrogen sorption on the resulting structures), such as V, Cr, Mn, Fe, Co, Ni. They showed that among considered 3*d* transition metals, Ni had the strongest bond with the GDY and the closest value of binding energy, E_{bind}, to cohesive energy of the metal atom in the crystal structure, E_{coh} (for V, Cr, Mn, Fe, Co, Ni they got $E_{bind} - E_{coh} = 3.3, 2.9, 1.8, 2.6, 2.1, 1.6$ eV, respectively). So, the formation of Ni clusters on the GDY surface is less probable, which is the desired scenario for hydrogen storage material, since metal clusters would decrease the resulting hydrogen uptake [20]. Therefore, for our investigation, we chose Ni-decorated GDY as a possible material for hydrogen storage. Moreover, though in He et al. work [19] the absolute value of Ni binding energy was big, it was lower than the experimental absolute value of Ni cohesion energy. Therefore, we also considered the influence of boron-doping on the performance of Ni-functionalized GDY, since this strategy proved its efficiency in enhancing the binding between light metal atoms and other 2D carbon nanomaterials (porous graphene [21], graphyne [22], and boron-graphdiyne [23]).

2. Models and simulation details

DFT spin-polarized calculations were performed using the projector-augmented wave (PAW) method [24] implemented in the Vienna Ab-initio Simulation Package (VASP) [25–27]. For exchange-correlation potential, we employed generalized gradient approximation (GGA) in Perdew-Burke-Ernzerhof (PBE) formalism. To account for van der Waals interactions, important for hydrogen adsorption energies estimation, we used DFT-D3 approach [28] throughout all calculations. Ground state geometries were obtained with $9 \times 9 \times 1$ Monkhorst-Pack set of *k*-points, the force convergence criteria of 10^{-3} eV/Å and the total energy convergence criteria in the self-consistent field iteration of 10^{-6} eV. The plane-wave basis set cut-off was 600 eV. With this set of parameters, the numerical precision of adsorption energies calculations is 3− 5 meV. We used the 2012 versions of pseudopotentials, constructed by the PAW method, which treat the following electrons as valence: $1s$ for H, $3d^8 4s^2$ for Ni, $2s^2 2p$ for B, and $2s^2 2p^2$ for C. Geometry relaxation was performed by conjugate-gradient method. Bader charge density analysis [29] was performed to calculate the atomic charges. And for relaxed structures, we performed calculations with the hybrid functional HSE06 [30] and fixed geometries to get more accurate DOS and charge transfer results, as standard GGA and LDA calculations give an underestimated bandgap. To investigate the thermal stability of boron-doped GDY, we also performed ab initio molecular dynamics (AIMD), using canonical NVT ensemble and Nose-Hoover thermostat implemented in VASP package. We utilized the PBE functional (with DFT-D3 corrections for vdW interactions) with the cut-off energy of 600 eV. The time step was 0.25 fs. We did not apply pressure to the system.

We investigated a single unit cell of the graphdiyne sheet, which contained eighteen carbon atoms (Fig. 1). In the non-periodic direction, we put 20 Å of vacuum, which was enough to exclude from the consideration the spurious interaction of the system with its image. The optimized cell parameters, as well as bond lengths of pure graphdiyne, are in agreement with the previously reported results [31,32]. In the case of boron-doped graphdiyne, we investigated a small concentration of boron (only one C atom per GDY unit cell was replaced). For a single unit cell of GDY, we added up to two Ni atoms. And for hydrogen adsorption, we considered up to five hydrogen molecules per Ni atom.

In the case of hydrogen adsorption on pristine graphdiyne, we also employed the SIESTA suite [34,35], in which wave function is expanded on the atomic basis set. It allowed us to perform a fast and precise test of a wide variety of hydrogen starting positions. We employed the generalized gradient approximation (Perdew-Burke-Ernzerhof functional [36]) and the local density approximation (Ceperley-Alder functional [37]) for obtaining the ground state geometries of a single hydrogen molecule adsorbed on the GDY. However, both these approximations do not account van der Waals (vdW) interactions (GGA usually results in the underestimated hydrogen adsorption energies, and LDA − overestimated [38,39]), so in the SIESTA package we also used the Grimme DFT-D2 corrections [40] and vdW exchange-correlation functional of Dion et al. [41] with exchange modified by K. Berland and P. Hyldgaard [42] for the most energetically favorable configuration, obtained from the GGA numerical experiments. For GGA (and DFT-D2) and LDA calculations, we used the pseudopotentials from the FHI pseudodatabase [43], for calculations with the vdW exchange-correlation functional we created pseudopotentials using ATOM package [44] and the GGA input file (.inp) from the FHI database. We have optimized the double-ζ polarized (DZP) basis set [45,46] for carbon and obtained the following parameters: for orbitals C^{2s} and C^{2p} cutoff radius is 8.0 and 9.6 Bohr, respectively, and Split-Norm is 0.35 and 0.20, respectively. Parameters for hydrogen atom were taken from our previous investigation [13]. Also, in binding energy calculations, we used counter-poise (CP) corrections by Boys and Bernardi to reduce basis set superposition error (BSSE), which can be significant in weakly interacted systems [47]. The mesh cutoff [48] of 350 and 210 Ry for GGA (and vdW) and LDA calculations, respectively, and $9 \times 9 \times 1$ Monkhorst-Pack set of *k*-points have been considered to calculate the total energies within a numerical precision of 1 meV. Geometry relaxation has been performed by the conjugate-gradient method with the force convergence criterion of $5 \cdot 10^{-5}$ Ry/Bohr. By the GDY total energy minimization, we obtained the equilibrium GDY lattice parameter: 9.48 and 9.39 Å for GGA and LDA calculations, respectively.

3. Results and discussion

3.1. B-doped GDY

We considered three symmetrically non-equivalent positions of B atom (Fig. 1, left side): one in the carbon ring (position B1) and two in the chain (positions B2 and B3). First, we optimized B-doped structures with the lattice parameters from pure GDY calculations. For the following investigation, we chose the structure with the lowest total energy, where boron is in the carbon ring (Fig. 1, right side), and obtained its optimal cell parameter. This parameter is bigger than that of pure graphdiyne since the original bond length being stretched by B substitution (B—C bond lengths are more than 6% larger than the corresponding C—C bond lengths), which agrees with the previous results for other carbon 2D allotropes: porous graphene [21] and graphyne [49]. The cohesive energy of B-doped GDY was calculated as follows

$$E_{coh} = \frac{E_{GDY@B} - n_C E_C - n_B E_B}{n_C + n_B}, \quad (1)$$

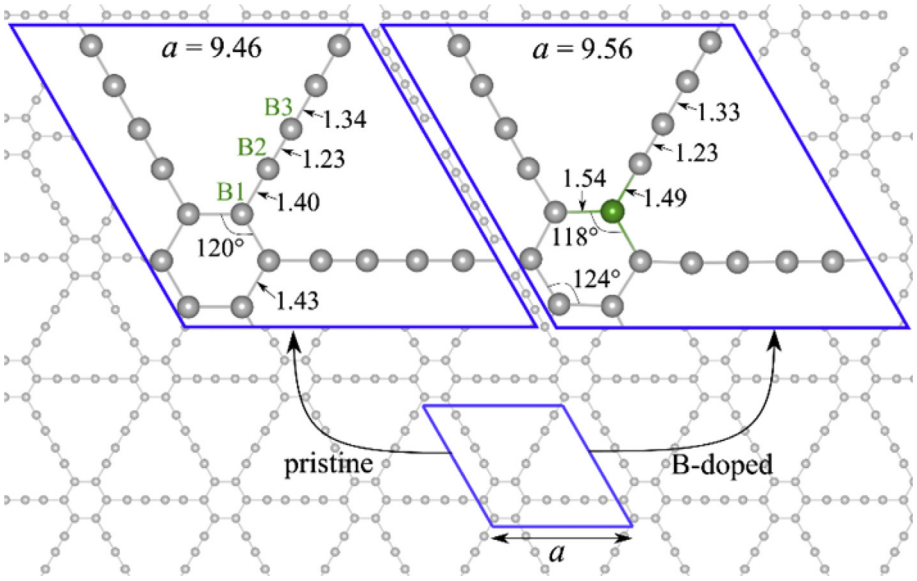

Fig. 1. Optimized structures of pristine and boron-doped graphdiyne. The unit cell is denoted by a blue line. Carbon and boron atoms are represented by gray and green color balls, respectively. All bond lengths and distances are in Å. All structure pictures were obtained using the VESTA3 software package [33].

where $E_{GDY@B}$ is the total energy of B-doped graphdiyne, E_C and E_B are the total energies of an isolated carbon and boron atom, respectively, and n_C and n_B are the number of carbon and boron atoms in the computational cell, respectively ($n_C = 17$, $n_B = 1$). We also estimated formation energy of GDY@B using the following formula:

$$E_{form} = \frac{E_{GDY@B} - n_C\mu_C - n_B\mu_B}{n_C + n_B}, \quad (2)$$

where μ_C is the total energy per carbon atom in pure GDY and μ_B is the total energy per boron atom in bulk β-R boron [50]. The resulting values for all considered B atom positions (B1-3) are presented in Table S1.

The calculated negative cohesive energy (−7.15 eV/atom in the case of B1 position), which is comparable to experimentally obtained value of graphite (−7.37 eV/atom [51]), indicates the stability of our B-doped graphdiyne system. However, positive formation energy (0.05 eV/atom for GDY@B1) indicates the endothermic B substitutional doping, which agrees with the previous results for graphyne [22]. We also tested the thermal stability of this system by performing ab initio MD calculation of four unit cells of GDY@B1 (68 carbon atoms, 4 boron atoms) at 300 K (Fig. S1). After 10 ps of an equilibration run and 5 ps of a production run, no breaking bonds and considerable geometry changes were observed, which implies the thermal stability of GDY@B at 300 K.

3.2. Ni decoration of pristine and B-doped GDY

At the next stage, we added one Ni atom per GDY supercell. Previously, He et al. [19] showed that the most stable position of Ni atom on graphdiyne is inside the big pore. So, we chose this position as a starting configuration. We also considered the other initial position of Ni atom, such as above the carbon hexagon ring. Geometrically relaxed structures are shown in Fig. 2. It can be seen that Ni decoration does not noticeably change the GDY(@B) structure if Ni is located above the carbon hexagon ring, and causes slight distortion of the carbon chain fragment (the shortest C≡C bond lengthens by more than 4%) if Ni is located in the big pore.

The binding energy of nickel adatoms was calculated as follows

$$E_{bind} = \frac{E_{GDY(@B)+Ni} - E_{GDY(@B)} - nE_{Ni}}{n}, \quad (3)$$

where $E_{GDY(@B)+Ni}$ is the total energy of graphdiyne structure (pristine or boron-doped) decorated by n Ni atoms, $E_{GDY(@B)}$ is the total energy of GDY (pristine or B-doped) without Ni, and E_{Ni} is the total energy of an isolated nickel atom. The resulting binding energies along with the Ni atom's Bader charges in the case of $n = 1$ are presented in Table 1.

Table 1 shows that doping with boron strengthens the binding between Ni adatom and the graphdiyne structure, especially when Ni is located above the carbon hexagon ring (the value of E_{bind} rises by 64% on GDY@B in comparison with the pristine GDY). This can be due to the increased charge transfer from Ni atom to the boron-doped GDY sheet (since boron atom lack one valence electron in comparison with carbon, enhancing the electron affinity of GDY structure) in comparison with the pristine one, which is indicated in Table 1 (Bader charge analysis of hybrid calculations) and shown in Fig. 2. Overall, binding of Ni atom to either pristine and boron-doped graphdiyne stems from the charge transfer and hybridization of Ni^{3d} and C^{2p} orbitals, which can be seen in Fig. 3. Fig. 3*a*, *b* shows that pristine GDY has a gap (0.90 eV in hybrid calculations and 0.48 eV in PBE calculations, which is close to the previous results [52]) in the density of states, which closes at boron doping. Subsequently, at Ni decoration, this small gap opens again in both pristine and B-doped graphdiyne.

Though obtained binding energies are quite big in value (especially in the case of "big pore" configuration of Ni atom), only in one position (in the big trigonal pore of GDY@B) Ni atom has binding energy slightly lower than the experimental value of $E_{coh}^{exp} = -4.44$ eV. This fact indicates the probability of Ni clusters formation at increasing concentration of metal atoms. It is not a desirable scenario, as clustering of active centers (Ni atoms, in our case) will reduce the possible hydrogen uptake [20,53].

We performed additional simulations with two Ni atoms in both pristine and B-doped GDY unit cells. Considered starting configurations (after structure relaxation) are denoted in Fig. S2. The average binding energies were calculated, using eq. (3) and applying $n = 2$. Obtained results (see Table S2) indicate that the

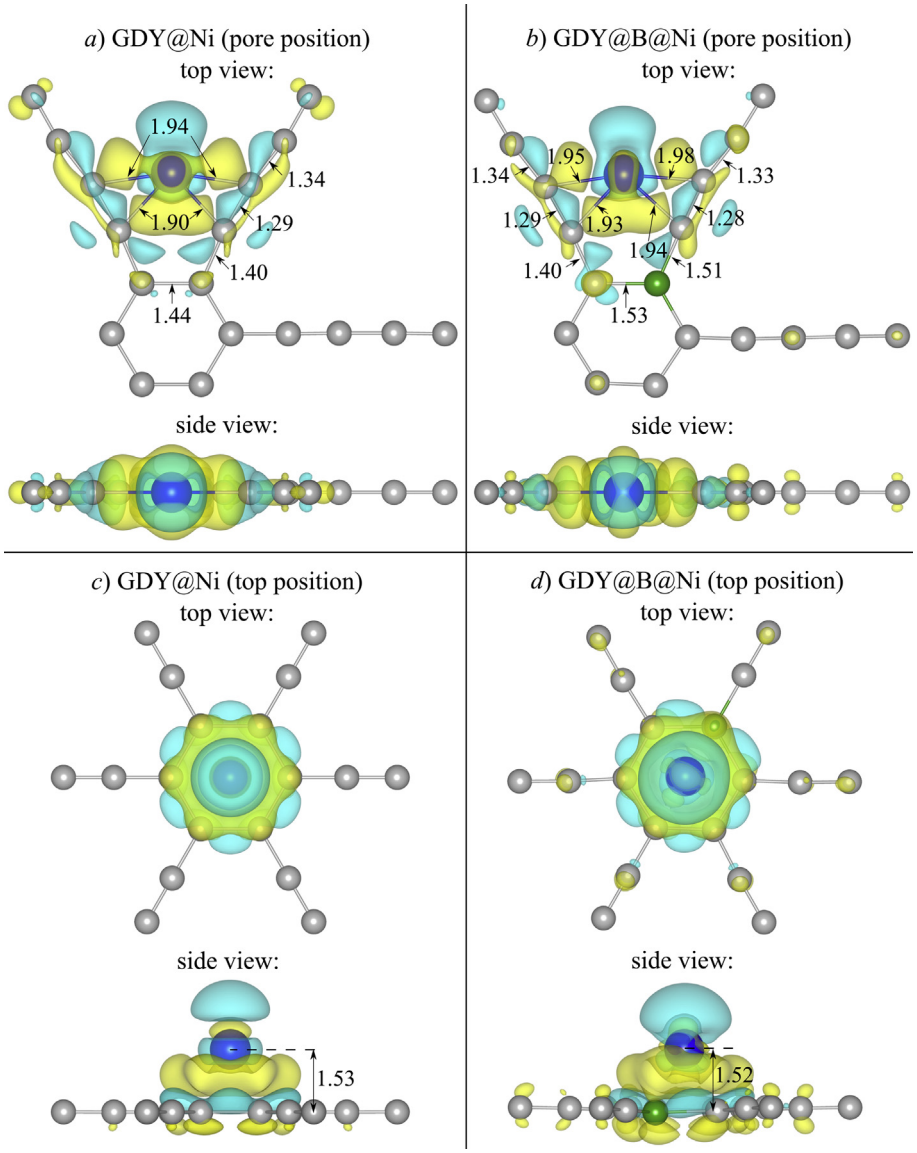

Fig. 2. Relaxed structures of pristine and B-doped GDY with Ni *a*) and *b*) inside the big pore; *c*) and *d*) on top of the small pore. Ni, C, and B atoms are blue, gray, and green, respectively. All bond lengths and distances are in Å. Cyan and yellow isosurfaces (0.0025 *e*) show charge depletion and accumulation, respectively.

Table 1
Binding energy and Bader charge of Ni atom on pristine and boron-doped graphdiyne.

Position of Ni atom	E_{bind}, eV	Q_{Bader} of Ni atom, *e*	
		DFT-D3 calculation	HSE06 calculation
Pristine GDY			
Big trigonal pore	−4.37	0.46	0.41
Hexagon top	−2.21	0.50	0.45
GDY@B			
Big trigonal pore	−4.48	0.53	0.65
Hexagon top	−3.68	0.54	0.66

configurations with a larger distance between Ni adatoms are more energetically favorable, which is due to the electrostatic repulsion between metal ions. So, cluster formation could be hindered by Coulomb interaction and would require passing a high potential barrier. However, further investigations, which are out of the scope of our research, are needed to clarify this point.

3.3. Hydrogen adsorption on pristine and Ni-functionalized GDY and GDY@B

On the next stage, we simulated hydrogen adsorption. We started by adding a single hydrogen molecule to pristine graphdiyne. A wide range of H_2 starting configurations (see Fig. S3) were optimized in SIESTA using the GGA and LDA approximations. The hydrogen adsorption energy was calculated as follows

$$E_{bind} = \frac{E_{base} + kE_{H_2} - E_{base+kH_2}}{k}, \quad (4)$$

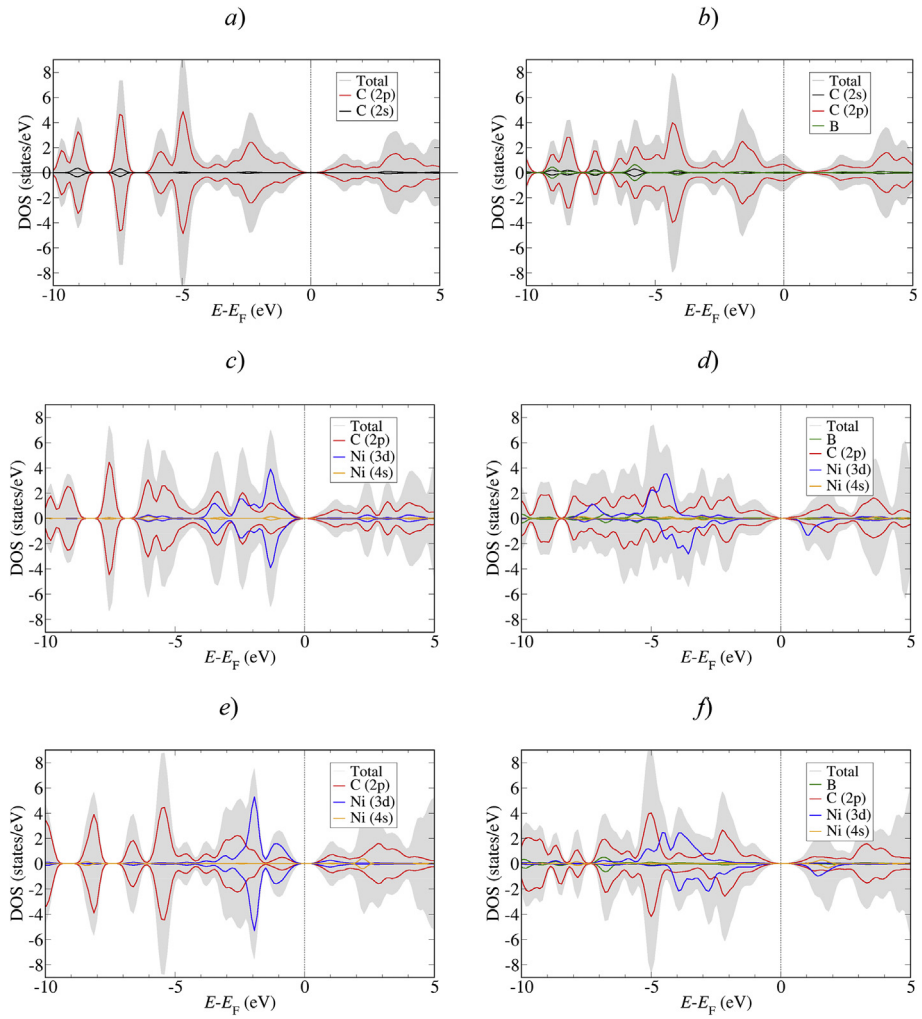

Fig. 3. Total and projected densities of states of *a*) pristine GDY (direct bandgap 0.90 eV); *b*) boron-doped GDY; *c*) GDY with Ni atom in the big pore (direct bandgap 0.59 eV); *d*) GDY@B with Ni atom in the big pore (direct bandgap 0.56 eV); *e*) GDY with Ni atom on top of carbon hexagon ring (direct bandgap 0.88 eV); *f*) GDY@B with Ni atom on top of the small pore (direct bandgap 0.84 eV). All DOS graphs and values of bandgap were obtained from the hybrid calculations.

where $E_{base+kH_2}$ is the total energy of the whole system (in this case, hydrogen molecule adsorbed on the GDY, so $k = 1$), E_{base} is the total energy of adsorbent (in this case, pristine GDY), and E_{H_2} is the total energy of an isolated hydrogen molecule. We used a "reversed" order of terms in eq. (4) to remove negative values in results. Here, positive E_{bind} indicates attractive interaction, and the bigger is its value the stronger is this attraction. The majority of the considered starting configuration transformed after geometry relaxation to the most energetically favorable ones, which are on top of the big trigonal and the small hexagonal pore, parallel to the GDY surface. Moreover, in GGA calculations we got negative $E_{bind} \approx -0.1$ eV for configurations located in the big pore (in the same plane as the GDY sheet), which agrees with the previous research [10].

The most energetically favorable configurations were subsequently simulated on pristine and boron-doped GDY using DFT-D3 corrections in VASP (also, for the sake of comparison, we performed additional calculations with Grimme DFT-D2 corrections and vdW exchange-correlation functional in SIESTA and Grimme DFT-D2 corrections in VASP; results of this modeling are given in Table S3). Not surprisingly, GGA gave the lowest adsorption energy (both in SIESTA and VASP calculations), and LDA – the highest. Different corrections (DFT-D2 and DFT-D3) and vdW exchange-correlation functional gave adsorption energies, which are between GGA and LDA values. Moreover, BSSE corrected results of SIESTA calculations are very close to energy values, obtained in VASP (if the same approach of treating the dispersion energy was used). Overall, the resulting adsorption energies are too low and out of the desired range of energies (200–600 meV per hydrogen molecule), which will enable effective hydrogen charging/recharging cycles [54,55].

Subsequently, we modeled hydrogen adsorption on Ni-functionalized GDY and GDY@B. For the configuration of Ni on top of the small pore, we considered up to five hydrogen molecules per Ni atom. However, only up to three H_2 molecules bound to the Ni@GDY(@B) complex. In the case of four and five hydrogen molecules, either extra (fourth and fifth) molecules went away from Ni atom or Ni atom formed a complex with three hydrogen molecules and went away from the graphdiyne (Fig. S4*b*,*c*). For the configuration of Ni atom in the big pore, we simulated only up to two hydrogen molecules per Ni atom, because even the second hydrogen molecule went away from the metal atom (Fig. S4*a*).

If Ni atom was on top of the small pore, because of the near-symmetrical form of the charge distribution of GDY(@B)@Ni, we chose symmetrical initial configurations of three H_2 molecules, which we have placed near the metal adatom. After that, we removed hydrogen molecules one by one with the structure

relaxation at each step. Also, for every number of H_2 molecules k, we removed a molecule from all possible symmetrically nonequivalent positions. For further analysis, we chose the structure with the minimal total energy. Optimized hydrogen configurations are shown in Fig. 4. During this "desorption" process (Fig. 4 $a \rightarrow c \rightarrow e$ for GDY and $b \rightarrow d \rightarrow f$ for GDY@B), Ni atom moved from position above the graphdiyne to the big tetragonal pore of GDY. This means that it is highly probable that even if GDY(@B)@Ni binds three hydrogen molecules per Ni atom, after the first sorption desorption cycle Ni atoms will move to the pore position and further will not take more than one hydrogen molecule.

We calculated average adsorption hydrogen energy using eq. (4). In this case, the adsorbent is the graphdiyne structure (pristine or boron-doped) functionalized by Ni atom. Using the same equation, we evaluated E_{bind}^{HSE} (energies were obtained by employing hybrid functional to the DFT-optimized structures without further geometry relaxation in HSE06 calculations).

However, for $k = 2, 3$ (Fig. 4*a-d*), the position of Ni atom differs from the equilibrium position of Ni atom on GDY(@B) (Fig. 2*c,d*). Therefore, we think, that to calculate hydrogen adsorption energy more correctly, we need to take the total energy of GDY(@B)@Ni complex with the geometry obtained from GDY(@B)Ni+kH_2 by removing hydrogen molecules (without geometry optimization, because if we let the system to move, Ni will go to the pore position as the most stable one). These "corrected" energies are noted as

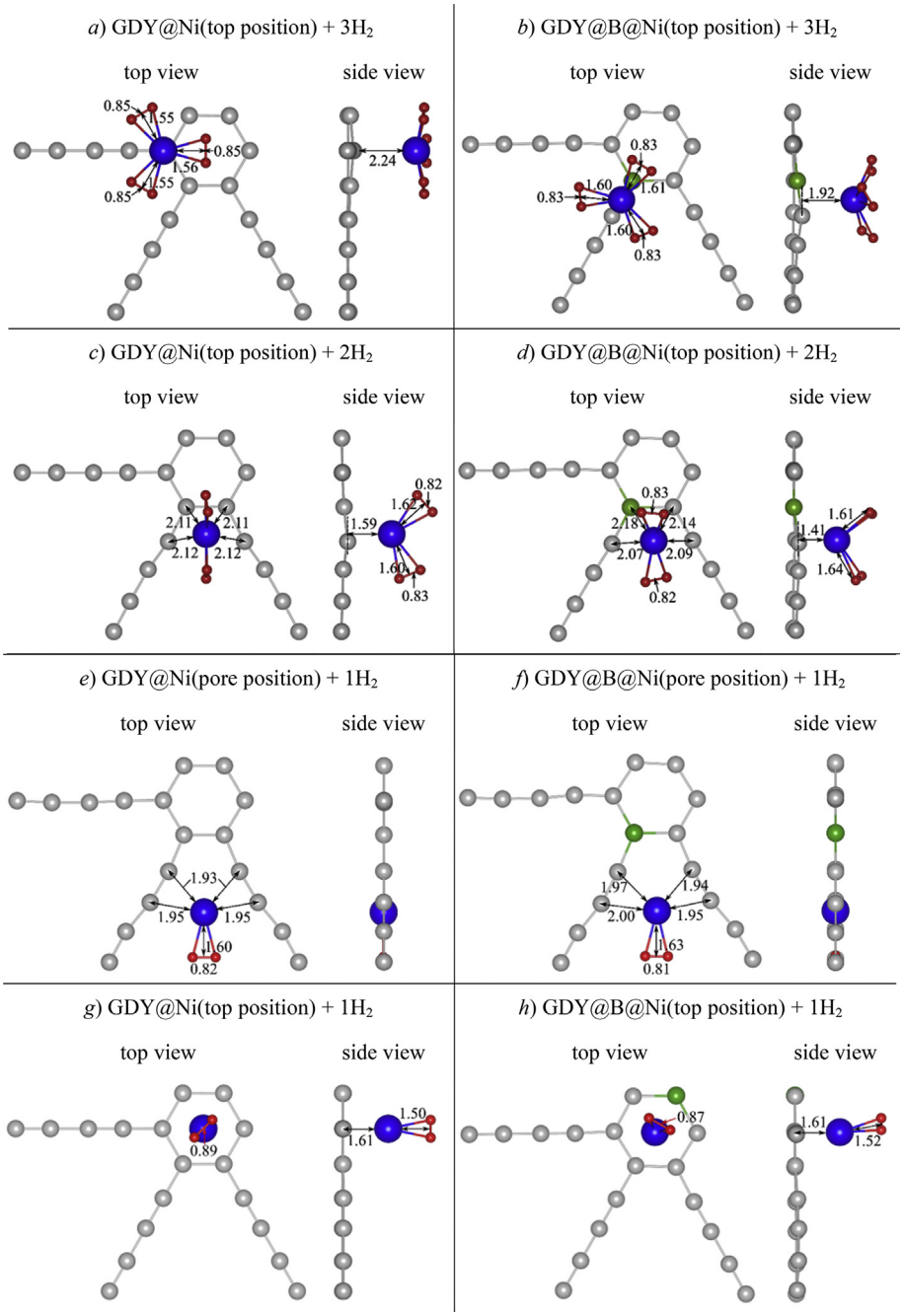

Fig. 4. Optimized structures of GDY@Ni + kH_2 and GDY@B@Ni + kH_2: *a*) and *b*) $k = 3$, top position of Ni; *c*) and *d*) $k = 2$, top position of Ni; *e*) and *f*) $k = 1$, pore position of Ni; *g*) and *h*) $k = 1$, top position of Ni. Carbon, boron, nickel and hydrogen atoms are gray, green, blue, and red, respectively. All bond lengths and distances are in Å.

E^{*}_{bind}. The results of adsorption energy calculations are presented in Table 2.

Table 2 shows that in the case of GDY@Ni only the configuration shown in Fig. 4*e* has the adsorption energy $E_{bind} = 666$ meV ($E^{HSE}_{bind} = 754$ meV) close to the desired energy range (200–600 meV per H_2 molecule). Other configurations have even higher adsorption energies with a maximum of 1.29 eV in the case of the structure presented in Fig. 4*g*. Such high binding energies stem from Kubas-type interaction [16] between H_2 molecules and Ni, which can be seen from the hybridization of the Ni *d*-orbital with the H *s*-orbital (Fig. S5) and the elongation of H–H bond. Moreover, in the case of $k = 3$ (Fig. 4*a*), high $E^{*}_{bind} = 950$ meV and the large distance between the Ni adatom and the GDY sheet (2.24 Å) suggest that Ni forms a complex with three hydrogen molecules, which then physically adsorbs to the graphdiyne. We modeled an isolated Ni@3H_2 complex and then calculated its binding energy to the GDY sheet as follows

$$E^{Ni@3H_2}_{bind} = E_{Ni@3H_2} + E_{GDY} - E_{GDY+Ni@3H_2}, \quad (5)$$

where $E_{Ni@3H_2}$ is the total energy of an isolated Ni@3H_2 complex, E_{GDY} is the total energy of the pristine GDY, and $E_{GDY+Ni@3H_2}$ is the total energy of the system GDY+Ni@3H_2. Here, again, because of the "reversed" order of terms positive binding energy means attraction. The resulting $E^{Ni@3H_2}_{bind} = 364$ meV corresponds to the physisorption, and it is 2.6 times lower than hydrogen $E^{*}_{bind} = 950$ meV. This suggests that increasing temperature during the desorption process will lead to the release of Ni@3H_2 complexes from the GDY, and not molecular hydrogen from GDY@Ni. By decreasing the vacuum region in the computational cell, we checked if a layered structure can solve this problem. The comparison of hydrogen adsorption energies and $E^{Ni@3H_2}_{bind}$ for different vacuum thickness is shown in Table S4. We can see that decreasing the distance between GDY sheets leads to the increase of $E^{Ni@3H_2}_{bind}$, but hydrogen E^{*}_{bind} increases at the same time remaining larger than $E^{Ni@3H_2}_{bind}$. Overall, Ni-functionalized GDY is not a good choice for hydrogen storage material since the obtained hydrogen binding energies are too high for room temperature applications.

Doping the graphdiyne with boron increases Ni binding to the GDY@B structure, in turn amending the hydrogen binding energies. First, E^{*}_{bind} significantly drops in the case of three hydrogen molecules: from 0.95 eV on GDY@Ni to 0.71 eV on GDY@B@Ni. And if we calculate $E^{Ni@3H_2}_{bind}$ on GDY@B, using eq. (5) with total energies of GDY@B, we will get 953 meV, which is higher than both corresponding $E^{*}_{bind} = 710$ meV and $E^{Ni@3H_2}_{bind} = 364$ meV on pure GDY. The enhanced binding between the Ni@3H_2 complex and GDY@B can also be seen from the charge density redistribution (Fig. S6). For the structure shown in Fig. 4*f* now we can get 0.53 eV (and even 0.38 eV in hybrid calculations) per H_2 molecule, which is in the desired energy range. In this case, we can estimate the desorption temperature at atmospheric pressure ($p = 1$ bar), using the van't Hoff equation:

$$T_D = \frac{E_{bind}}{k_B}\left(\frac{\Delta S}{R}\right)^{-1}, \quad (6)$$

where E_{bind} is hydrogen adsorption energy, k_B is Boltzmann constant, ΔS is the change in hydrogen entropy from gas to a liquid phase, R is gas constant. Using ΔS from [56], we obtained $T_D = 446$ K for $E_{bind} = 531$ meV (and $T_D = 318$ K for $E^{HSE}_{bind} = 379$ meV). These desorption temperature estimations are very promising for room temperature applications, however, we should also pay attention to the hydrogen uptake. H_2 gravimetric density GD_H could be estimated as

$$GD_H = \frac{2 \times W_H \times n}{N_C \times W_C + W_B + W_{Ni} \times n + 2 \times W_H \times n}, \quad (7)$$

where W represents the corresponding atomic weight, N_C is the number of carbon atoms in the computational cell ($N_C = 17$), n is the number of Ni atoms in the computational cell (we assume we have one hydrogen molecule per Ni adatom, since only in this case we have hydrogen adsorption energies in the needed range). The resulting GD_H for the structure shown in Fig. 4*f* is too low, only 0.7 wt %. Even if we consider two Ni atoms in the computational cell (Fig. S2*d*,*e*), we will get only 1.2 wt %.

Even though our resulting hydrogen uptake is lower than the U.S. DOE target, it is still bigger than for other carbon-based nanomaterials. First, though theoretical investigations showed, that on graphene, another 2D carbon allotrope, each Ni adatom can adsorb up to two [57] and even four [58] hydrogen molecules with the adsorption energy in the desired range of 200–600 meV/H_2, the E_{bind} of Ni and graphene is lower in absolute value than the Ni E_{coh}, which indicates the high possibility of Ni clusters formation. Indeed, another theoretical research [59] showed that Ni clusters are energetically favorable even on the defective graphene, and the resulting hydrogen uptake is 0.3 wt % (this evaluation was obtained for H_2 molecules with adsorption energy larger than 200 meV). This result complies with the experimental investigations of hydrogen adsorption by graphene decorated with Ni nanoparticles (NP): Gaboardi et al. [60] got hydrogen uptake of 1.1 wt % at 77 K and 1 bar; Zhou et al. [61] got 0.14 wt % at room temperature and 1 bar and 1.18 wt % at room temperature and 60 bar. A similar situation was observed with carbon nanotubes (CNTs): according to DFT simulations, an isolated Ni atom can adsorb 2–3 H_2 molecules with energies close to 600 meV/H_2 but Ni binding energies are low [62]. The experimental investigation of multi-walled CNTs [63] showed that after Ni decoration they can adsorb only 0.6 wt % of hydrogen. Even lower hydrogen uptakes were observed for reduced graphene oxide decorated with Ni NP: 0.007 wt % at 293 K and 1 bar [64], and 0.24 wt % at 300 K and 20 bar [65]. The promising theoretical results were obtained for fullerenes: two out of five H_2 molecules adsorbed by an isolated Ni atom on the C_{60} have adsorption energies in the desired range, and upon the boron substitution this number rose to four [66]. However, Ni binding energy was lower than the cohesive energy, and Ni clustering was not investigated in detail, so it is

Table 2
Average hydrogen adsorption energies on Ni-functionalized GDY and GDY@B

Ni position	*k*	GDY			GDY@B		
		E_{bind}, eV	E^{HSE}_{bind}, eV	E^{*}_{bind}, eV	E_{bind}, eV	E^{HSE}_{bind}, eV	E^{*}_{bind}, eV
top	1	1.294	1.178	–	1.060	0.814	–
	2	0.894	0.687	0.722	0.842	0.703	0.671
	3	0.654	0.583	0.950	0.574	0.286	0.710
pore	1	0.666	0.754	–	0.531	0.379	–

hard to estimate the hydrogen uptake without further investigations.

4. Conclusions

In this work, we have systematically studied pristine, boron-doped, and Ni-decorated graphdiyne and their interaction with molecular hydrogen within the DFT framework. The electronic structure and charge density distributions were analyzed using PBE and hybrid (HSE06) functionals. The effect of vdW dispersion was assessed by utilization GGA (PBE functional), LDA (CA functional), vdW-BH functional, Grimme DFT-D2 and DFT-D3 corrections. We showed that though doping the GDY with boron atoms at small concentrations is an endothermic process, the resulting structure is thermally stable at least at room temperature. For pristine and B-doped GDY we got too small hydrogen binding energies (~70 meV per H_2 molecule in DFT-D3 calculations), which suggests that without more active adsorption sites GDY (both pristine and B-doped) can serve as a hydrogen storage media only at cryogenic temperatures.

To enhance the binding between hydrogen and graphdiyne, we functionalized the latter with Ni atoms. We found two stable positions of TM adatom (on top of the small hexagonal pore and in the big trigonal pore, the latter is more energetically favorable). Boron doping enhances the binding between Ni adatom and the graphdiyne structure (especially when Ni is located above the small hexagonal pore) due to the increased charge transfer from Ni atom to the boron-doped GDY sheet in comparison with the pristine one. However, only in one position (in the big trigonal pore of GDY@B), Ni atom has binding energy lower than the experimental value.

Adding Ni induce a huge increase of hydrogen binding energies in comparison of pristine and B-doped GDY (up to 1.29 eV per H_2 molecule). Overall, GDY@Ni binds hydrogen with the energy too high for room-temperature applications. Doping with boron improves the energies, and on GDY@B@Ni the evaluation of desorption temperature is ~300–500 K. However, it turned out that one Ni atom can reversibly bind only one hydrogen molecule, which results in low reversible hydrogen uptake, only ~1.2 wt %. To summarize, though Ni-functionalized GDY has good estimations for hydrogen desorption temperature, it cannot reach the U.S. DOE target of gravimetric density. However, boron-doping could be an effective strategy to decrease too high hydrogen binding energies and could be implemented for functionalization with other transition metals.

Declaration of Competing Interest

The authors declare no competing financial interest.

Acknowledgements

A.B. and R.A. acknowledge respectively the Carl Tryggers Stiftelse for Vetenskaplig Forskning (CTS: Grant 18.04) and Swedish Research Council (VR Grant 2016–06014). E.A. is thankful for the Swedish Institute for providing a scholarship for her internship at Uppsala University. SUSU SSL (Tornado SUSU Supercomputer), SNIC, and HPC2N are also acknowledged for providing computing time.

Appendix A. Supplementary data

Supplementary data to this article can be found online at https://doi.org/10.1016/j.mtener.2020.100421.

References

[1] S. Dutta, A review on production, storage of hydrogen and its utilization as an energy resource, J. Ind. Eng. Chem. 20 (4) (2014) 1148–1156, https://doi.org/10.1016/j.jiec.2013.07.037.
[2] K. Mazloomi, C. Gomes, Hydrogen as an energy carrier: prospects and challenges, Renew. Sustain. Energy Rev. 16 (5) (2012) 3024–3033, https://doi.org/10.1016/j.rser.2012.02.028.
[3] DOE technical targets for onboard hydrogen storage for light-duty vehicles. https://www.energy.gov/eere/fuelcells/doe-technical-targets-onboard-hydrogen-storage-light-duty-vehicles. (Accessed 20 January 2020).
[4] Y.M. Manawi, Ihsanullah, A. Samara, T. Al-Ansari, M.A. Atieh, Review of carbon nanomaterials' synthesis via the chemical vapor deposition (CVD) method, Materials 11 (5) (2018) 36, https://doi.org/10.3390/ma11050822.
[5] M. Mohan, V.K. Sharma, E.A. Kumar, V. Gayathri, Hydrogen storage in carbon materials—a review, Energy Storage (2019) e35, https://doi.org/10.1002/est2.35.
[6] Y.D. Xia, Z.X. Yang, Y.Q. Zhu, Porous carbon-based materials for hydrogen storage: advancement and challenges, J. Mater. Chem. A 1 (33) (2013) 9365–9381, https://doi.org/10.1039/c3ta10583k.
[7] C.N. Ge, J. Chen, S.L. Tang, Y.W. Du, N.J. Tang, Review of the electronic, optical, and magnetic properties of graphdiyne: from theories to experiments, ACS Appl. Mater. Interfaces 11 (3) (2019) 2707–2716, https://doi.org/10.1021/acsami.8b03413.
[8] G.X. Li, Y.L. Li, H.B. Liu, Y.B. Guo, Y.J. Li, D.B. Zhu, Architecture of graphdiyne nanoscale films, Chem. Commun. 46 (19) (2010) 3256–3258, https://doi.org/10.1039/b922733d.
[9] Y.P. Zheng, Y.H. Chen, L.H. Lin, Y.Y. Sun, H.B. Liu, Y.L. Li, Y.W. Du, N.J. Tang, Intrinsic magnetism of graphdiyne, Appl. Phys. Lett. 111 (3) (2017) 5, https://doi.org/10.1063/1.4993916.
[10] M. Bartolomei, E. Carmona-Novillo, G. Giorgi, First principles investigation of hydrogen physical adsorption on graphynes' layers, Carbon 95 (2015) 1076–1081, https://doi.org/10.1016/j.carbon.2015.08.118.
[11] P. Panigrahi, A.K. Dhinakaran, S.R. Naqvi, S.R. Gollu, R. Ahuja, T. Hussain, Light metal decorated graphdiyne nanosheets for reversible hydrogen storage, Nanotechnology 29 (35) (2018) 10, https://doi.org/10.1088/1361-6528/aac84c.
[12] M. Ebadi, A. Reisi-Vanani, F. Houshmand, P. Amani, Calcium-decorated graphdiyne as a high hydrogen storage medium: evaluation of the structural and electronic properties, Int. J. Hydrogen Energy 43 (52) (2018) 23346–23356, https://doi.org/10.1016/j.ijhydene.2018.10.205.
[13] E. Anikina, A. Banerjee, V. Beskachko, R. Ahuja, Li-functionalized carbon nanotubes for hydrogen storage: importance of size effects, ACS Appl. Nano Mater. 2 (5) (2019) 3021–3030, https://doi.org/10.1021/acsanm.9b00406.
[14] E. Anikina, A. Banerjee, V. Beskachko, R. Ahuja, Li-decorated carbyne for hydrogen storage: charge induced polarization and van't Hoff hydrogen desorption temperature, Sustain. Energy Fuels 4 (2020) 691–699, https://doi.org/10.1039/C9SE00706G.
[15] C.Q. Xiang, A. Li, S.L. Yang, Z.G. Lan, W. Xie, Y.M. Tang, H.X. Xu, Z. Wang, H.S. Gu, Enhanced hydrogen storage performance of graphene nanoflakes doped with Cr atoms: a DFT study, RSC Adv. 9 (44) (2019) 25690–25696, https://doi.org/10.1039/c9ra04589a.
[16] C.V.J. Skipper, T.K.A. Hoang, D.M. Antonelli, N. Kaltsoyannis, Transition metal hydrazide-based hydrogen-storage materials: the first atoms-in-molecules analysis of the Kubas interaction, Chem. Eur. J. 18 (6) (2012) 1750–1760, https://doi.org/10.1002/chem.201102715.
[17] G.J. Kubas, Hydrogen activation on organometallic complexes and H2 production, utilization, and storage for future energy, J. Organomet. Chem. 694 (17) (2009) 2648–2653, https://doi.org/10.1016/j.jorganchem.2009.05.027.
[18] T. Yildirim, S. Ciraci, Titanium-decorated carbon nanotubes as a potential high-capacity hydrogen storage medium, Phys. Rev. Lett. 94 (17) (2005), https://doi.org/10.1103/PhysRevLett.94.175501.
[19] J.J. He, S.Y. Ma, P. Zhou, C.X. Zhang, C.Y. He, L.Z. Sun, Magnetic properties of single transition-metal atom absorbed graphdiyne and graphyne sheet from DFT plus U calculations, J. Phys. Chem. C 116 (50) (2012) 26313–26321, https://doi.org/10.1021/jp307408u.
[20] P.O. Krasnov, F. Ding, A.K. Singh, B.I. Yakobson, Clustering of Sc on SWNT and reduction of hydrogen uptake: ab-initio all-electron calculations, J. Phys. Chem. C 111 (49) (2007) 17977–17980, https://doi.org/10.1021/jp077264t.
[21] R.F. Lu, D.W. Rao, Z.L. Lu, J.C. Qian, F. Li, H.P. Wu, Y.Q. Wang, C.Y. Xiao, K.M. Deng, E.J. Kan, W.Q. Deng, Prominently improved hydrogen purification and dispersive metal binding for hydrogen storage by substitutional doping in porous graphene, J. Phys. Chem. C 116 (40) (2012) 21291–21296, https://doi.org/10.1021/jp308195m.
[22] R.F. Lu, D.W. Rao, Z.S. Meng, X.B. Zhang, G.J. Xu, Y.Z. Liu, E.J. Kan, C.Y. Xiao, K.M. Deng, Boron-substituted graphyne as a versatile material with high storage capacities of Li and H-2: a multiscale theoretical study, Phys. Chem. Chem. Phys. 15 (38) (2013) 16120–16126, https://doi.org/10.1039/c3cp52364k.
[23] T. Hussain, B. Mortazavi, H. Bae, T. Rabczuk, H. Lee, A. Karton, Enhancement in hydrogen storage capacities of light metal functionalized Boron-Graphdiyne nanosheets, Carbon 147 (2019) 199–205, https://doi.org/10.1016/j.carbon.2019.02.085.

[24] G. Kresse, D. Joubert, From ultrasoft pseudopotentials to the projector augmented-wave method, Phys. Rev. B 59 (3) (1999) 1758–1775, https://doi.org/10.1103/PhysRevB.59.1758.
[25] G. Kresse, J. Hafner, Abinitio molecular-dynamics for liquid-metals, Phys. Rev. B 47 (1) (1993) 558–561, https://doi.org/10.1103/PhysRevB.47.558.
[26] G. Kresse, J. Furthmuller, Efficiency of ab-initio total energy calculations for metals and semiconductors using a plane-wave basis set, Comput. Mater. Sci. 6 (1) (1996) 15–50, https://doi.org/10.1016/0927-0256(96)00008-0.
[27] G. Kresse, J. Furthmuller, Efficient iterative schemes for ab initio total-energy calculations using a plane-wave basis set, Phys. Rev. B 54 (16) (1996) 11169–11186, https://doi.org/10.1103/PhysRevB.54.11169.
[28] S. Grimme, J. Antony, S. Ehrlich, H. Krieg, A consistent and accurate ab initio parametrization of density functional dispersion correction (DFT-D) for the 94 elements H-Pu, J. Chem. Phys. 132 (15) (2010) 19, https://doi.org/10.1063/1.3382344.
[29] G. Henkelman, A. Arnaldsson, H. Jonsson, A fast and robust algorithm for Bader decomposition of charge density, Comput. Mater. Sci. 36 (3) (2006) 354–360, https://doi.org/10.1016/j.commatsci.2005.04.010.
[30] A.V. Krukau, O.A. Vydrov, A.F. Izmaylov, G.E. Scuseria, Influence of the exchange screening parameter on the performance of screened hybrid functionals, J. Chem. Phys. 125 (22) (2006) 5, https://doi.org/10.1063/1.2404663.
[31] C.S. Huang, Y.J. Li, N. Wang, Y.R. Xue, Z.C. Zuo, H.B. Liu, Y.L. Li, Progress in research into 2D graphdiyne-based materials, Chem. Rev. 118 (16) (2018) 7744–7803, https://doi.org/10.1021/acs.chemrev.8b00288.
[32] M.Q. Long, L. Tang, D. Wang, Y.L. Li, Z.G. Shuai, Electronic structure and carrier mobility in graphdiyne sheet and nanoribbons: theoretical predictions, ACS Nano 5 (4) (2011) 2593–2600, https://doi.org/10.1021/nn102472s.
[33] K. Momma, F. Izumi, VESTA 3 for three-dimensional visualization of crystal, volumetric and morphology data, J. Appl. Crystallogr. 44 (2011) 1272–1276, https://doi.org/10.1107/s0021889811038970.
[34] J.M. Soler, E. Artacho, J.D. Gale, A. Garcia, J. Junquera, P. Ordejon, D. Sanchez-Portal, The SIESTA method for ab initio order-N materials simulation, J. Phys. Condens. Matter 14 (11) (2002) 2745–2779, https://doi.org/10.1088/0953-8984/14/11/302.
[35] P. Ordejon, E. Artacho, J.M. Soler, Self-consistent order-N density-functional calculations for very large systems, Phys. Rev. B 53 (16) (1996) 10441–10444, https://doi.org/10.1103/PhysRevB.53.R10441.
[36] J.P. Perdew, K. Burke, M. Ernzerhof, Generalized gradient approximation made simple, Phys. Rev. Lett. 77 (18) (1996) 3865–3868, https://doi.org/10.1103/PhysRevLett.77.3865.
[37] D.M. Ceperley, B.J. Alder, Ground-state of the electron-gas by a stochastic method, Phys. Rev. Lett. 45 (7) (1980) 566–569, https://doi.org/10.1103/PhysRevLett.45.566.
[38] I. Cabria, M.J. Lopez, J.A. Alonso, Searching for DFT-based methods that include dispersion interactions to calculate the physisorption of H-2 on benzene and graphene, J. Chem. Phys. 146 (21) (2017) 11, https://doi.org/10.1063/1.4984106.
[39] J. Klimes, A. Michaelides, Perspective: advances and challenges in treating van der Waals dispersion forces in density functional theory, J. Chem. Phys. 137 (12) (2012) 120901, https://doi.org/10.1063/1.4754130.
[40] S. Grimme, Semiempirical GGA-type density functional constructed with a long-range dispersion correction, J. Comput. Chem. 27 (15) (2006) 1787–1799, https://doi.org/10.1002/jcc.20495.
[41] M. Dion, H. Rydberg, E. Schroder, D.C. Langreth, B.I. Lundqvist, Van der Waals density functional for general geometries, Phys. Rev. Lett. 92 (24) (2004) 4, https://doi.org/10.1103/PhysRevLett.92.246401.
[42] K. Berland, P. Hyldgaard, Exchange functional that tests the robustness of the plasmon description of the van der Waals density functional, Phys. Rev. B 89 (3) (2014) 8, https://doi.org/10.1103/PhysRevB.89.035412.
[43] Abinit's Fritz-Haber-Institute (FHI) pseudo database. https://departments.icmab.es/leem/SIESTA_MATERIAL/Databases/Pseudopotentials/periodictable-intro.html. (Accessed 15 June 2019).
[44] ATOM, a program for DFT calculations in atoms and pseudopotential generation, maintained by Alberto Garcia. https://departments.icmab.es/leem/SIESTA_MATERIAL/Pseudos/Code/downloads.html. (Accessed 15 June 2019).
[45] E. Anglada, J.M. Soler, J. Junquera, E. Artacho, Systematic generation of finite-range atomic basis sets for linear-scaling calculations, Phys. Rev. B 66 (20) (2002) 4, https://doi.org/10.1103/PhysRevB.66.205101.
[46] J. Junquera, O. Paz, D. Sanchez-Portal, E. Artacho, Numerical atomic orbitals for linear-scaling calculations, Phys. Rev. B 64 (23) (2001) 9, https://doi.org/10.1103/PhysRevB.64.235111.
[47] K. Lee, J.J. Yu, Y. Morikawa, Comparison of localized basis and plane-wave basis for density-functional calculations of organic molecules on metals, Phys. Rev. B 75 (4) (2007) 5, https://doi.org/10.1103/PhysRevB.75.045402.
[48] E. Artacho, D. Sanchez-Portal, P. Ordejon, A. Garcia, J.M. Soler, Linear-scaling ab-initio calculations for large and complex systems, Phys. Status Solidi B Basic Solid State Phys. 215 (1) (1999) 809–817, https://doi.org/10.1002/(sici)1521-3951(199909)215:1<809::aid-pssb809>3.0.co;2-0.
[49] B. Bhattacharya, U. Sarkar, The effect of boron and nitrogen doping in electronic, magnetic, and optical properties of graphyne, J. Phys. Chem. C 120 (47) (2016) 26793–26806, https://doi.org/10.1021/acs.jpcc.6b07478.
[50] O.O. Kurakevych, V.L. Solozhenko, Rhombohedral boron subnitride, B13N2, by X-ray powder diffraction, Acta Crystallogr. Section C Struct. Chem. 63 (2007) I80–I82, https://doi.org/10.1107/s0108270107037353.
[51] X. Jiang, C. Arhammar, P. Liu, J.J. Zhao, R. Ahuja, The R3-carbon allotrope: a pathway towards glassy carbon under high pressure, Sci. Rep. 3 (2013) 9, https://doi.org/10.1038/srep01877.
[52] K. Srinivasu, S.K. Ghosh, Graphyne and graphdiyne: promising materials for nanoelectronics and energy storage applications, J. Phys. Chem. C 116 (9) (2012) 5951–5956, https://doi.org/10.1021/jp212181h.
[53] Q. Sun, Q. Wang, P. Jena, Y. Kawazoe, Clustering of Ti on a C-60 surface and its effect on hydrogen storage, J. Am. Chem. Soc. 127 (42) (2005) 14582–14583, https://doi.org/10.1021/ja0550125.
[54] Y.H. Kim, Y.F. Zhao, A. Williamson, M.J. Heben, S.B. Zhang, Nondissociative adsorption of H-2 molecules in light-element-doped fullerenes, Phys. Rev. Lett. 96 (1) (2006) 4, https://doi.org/10.1103/PhysRevLett.96.016102.
[55] J. Li, T. Furuta, H. Goto, T. Ohashi, Y. Fujiwara, S. Yip, Theoretical evaluation of hydrogen storage capacity in pure carbon nanostructures, J. Chem. Phys. 119 (4) (2003) 2376–2385, https://doi.org/10.1063/1.1582831.
[56] E. Lemmon, in: W.M. Haynes, et al. (Eds.), Handbook of Chemistry and Physics, 96th edn, CRC Press, 2016, pp. 21–37. Section 6.
[57] J. Wong, S. Yadav, J. Tam, C.V. Singh, A van der Waals density functional theory comparison of metal decorated graphene systems for hydrogen adsorption, J. Appl. Phys. 115 (22) (2014) 11, https://doi.org/10.1063/1.4882197.
[58] A. Sigal, M.I. Rojas, E.P.M. Leiva, Interferents for hydrogen storage on a graphene sheet decorated with nickel: a DFT study, Int. J. Hydrogen Energy 36 (5) (2011) 3537–3546, https://doi.org/10.1016/j.ijhydene.2010.12.024.
[59] C.M. Ramos-Castillo, J.U. Reveles, M.E. Cifuentes-Quintal, R.R. Zope, R. de Coss, Ti-4- and Ni-4-Doped defective graphene nanoplatelets as efficient materials for hydrogen storage, J. Phys. Chem. C 120 (9) (2016) 5001–5009, https://doi.org/10.1021/acs.jpcc.5b12711.
[60] M. Gaboardi, A. Bliersbach, G. Bertoni, M. Aramini, G. Vlahopoulou, D. Pontiroli, P. Mauron, G. Magnani, G. Salviati, A. Zuttel, M. Ricco, Decoration of graphene with nickel nanoparticles: study of the interaction with hydrogen, J. Mater. Chem. A 2 (4) (2014) 1039–1046, https://doi.org/10.1039/c3ta14127f.
[61] C.Y. Zhou, J.A. Szpunar, X.Y. Cui, Synthesis of Ni/graphene nanocomposite for hydrogen storage, ACS Appl. Mater. Interfaces 8 (24) (2016) 15232–15241, https://doi.org/10.1021/acsami.6b02607.
[62] M.Y. Ni, X.L. Wang, Z. Zeng, Interaction of hydrogen molecules on Ni-doped single-walled carbon nanotube, Chin. Phys. B 18 (1) (2009) 357–362.
[63] M. Mehrabi, A. Reyhani, P. Parvin, S.Z. Mortazavi, Surface structural alteration of multi-walled carbon nanotubes decorated by nickel nanoparticles based on laser ablation/chemical reduction methods to enhance hydrogen storage properties, Int. J. Hydrogen Energy 44 (7) (2019) 3812–3823, https://doi.org/10.1016/j.ijhydene.2018.12.122.
[64] L. Wei, Y.B. Mao, Enhanced hydrogen storage performance of reduced graphene oxide hybrids with nickel or its metallic mixtures based on spillover mechanism, Int. J. Hydrogen Energy 41 (27) (2016) 11692–11699, https://doi.org/10.1016/j.ijhydene.2016.04.030.
[65] N. Ismail, M. Madian, M.S. El-Shall, Reduced graphene oxide doped with Ni/Pd nanoparticles for hydrogen storage application, J. Ind. Eng. Chem. 30 (2015) 328–335, https://doi.org/10.1016/j.jiec.2015.06.002.
[66] S. Awasthi, S.K. Pandey, C.P. Pandey, K. Balani, Progress in electrochemical and electrophoretic deposition of nickel with carbonaceous allotropes: a review, Adv. Mater. Interfaces 7 (1) (2020) 33, https://doi.org/10.1002/admi.201901096.